Structural Origin of Corrosion Inhibition Effect over 2-(2-Hydroxyphenyl)benzothiazole on Steel in HCl Medium

Shenying Xu[1,2], Wenpo Li[1,], Xiuli Zuo[3], Dongdong Zheng[1], Xingwen Zheng[1,4], Shengtao Zhang[1]*

[1] School of Chemistry and Chemical Engineering, Chongqing University, Chongqing 400044, PR China
[2] School of Chemistry and Chemical Engineering, Yibin University, Yinbin 644000, PR China
[3] Department of Oil Application & Management Engineering, Logistic Engineering University, Chongqing 401331, PR China
[4] School of Chemical and Pharmaceutical Engineering, Sichuan University of Science & Engineering, Zigong 643000, PR China
[*] E-mail: cqwpli@126.com

The inhibition effect of 2-(2-Hydroxyphenyl)benzothiazole (HBT), a newly synthesized benzothiazole derivative, on mild steel in 1 M HCl medium has been investigated by utilizing weight loss measurements, electrochemical methods and morphology characterization. The results indicate that HBT exhibited a superior corrosion inhibition efficiency, which reached approximately 95% with the addition of 0.07 mM HBT. Electrochemical tests illustrate that HBT is a mixed-type inhibitor. According to the Langmuir adsorption isotherm, the thermodynamic and kinetic parameters of the adsorption process complied with a physical-adsorption mechanism. Furthermore, computational calculations based on density functional theory reveal the relation between the electronic properties and the inhibition efficiency. In combination with the value of pK_a, the protonic form of HBT in corrosive medium was predicted.

1. INTRODUCTION

The addition of corrosion inhibitors has been proven to be one of the most efficient ways to protect mild steel from corrosion during chemical cleaning [1, 2]. In recent years, numerous organic compounds containing N, P, S and O atoms have been proven to function as excellent inhibitors by forming a protective layer in the aggressive medium [3-6]. Otherwise, the adsorption ability of the

compounds on steel surfaces is mainly related to π-electrons and lone-pair electrons [7-9]. Thus, benzothiazole and its derivatives are considered to be promising inhibitors due to the existence of heteroatoms (N, O, S) and aromatic rings in their structures [10-14]. 2-(2-Hydroxyphenyl)benzothiazole (HBT), as shown in Fig. 1, has a larger molecular weight and volume than benzothiazole, leading to higher surface coverage when the inhibitor adsorbs on mild steel [15, 16]. Moreover, the hydroxy in HBT increases the solubility in the studied solvent. However, there are insufficient studies on HBT as an inhibitor for mild steel in corrosive solution.

In this study, we aim to probe the performance of HBT as a corrosion inhibitor for mild steel in 1 M HCl by using multiple techniques. The thermodynamic and kinetic parameters are researched at various temperatures. In addition, the interaction mechanism between HBT and steel is revealed by theoretical calculations based on density functional theory.

2. EXPERIMENTAL

2.1. Materials and sample preparation

HBT (98 wt.%), as the tested inhibitor, was purchased from the Aladdin Company. Corrosive medium (1 M HCl) was prepared by the dilution of analytical reagent grade 37% HCl with distilled water. The chemical composition of mild steel was C (0.16 wt.%), Si (0.24 wt.%), Mn (0.43 wt.%), P (0.049 wt.%), S (0.015 wt.%) and Fe. The sizes of the specimens were 10 mm × 20 mm × 30 mm and 10 mm × 10 mm × 10 mm for weight loss tests and electrochemical measurements, respectively. Meanwhile, the samples for electrochemical measurements were embedded in epoxy, leaving one side as the working area after being polished by emery paper of up to 1200 grit. Before each measurement, all specimens were cleaned by acetone and distilled water, then dried at room temperature. A water thermostat with an accuracy of 1 K was used to control the temperature of the solution during measurements. All experiments were performed under ambient conditions.
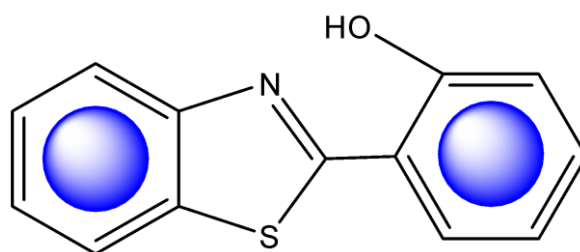

Figure 1. Molecular structure of HBT.

2.2. Weight loss measurements

The specimens were immersed in 1 M HCl solution with various HBT concentrations for 4 h at 298, 308, 318, and 328 K, respectively. Afterwards, they were removed and rinsed with distilled water and acetone. The mass losses of the samples were calculated based on the weight before and after

immersion. Three parallel tests were conducted in each condition for obtaining the average value of corrosion rate (CR).

2.3. Electrochemical measurements

Electrochemical experiments were performed by a three-electrode system on a CHI660B electrochemical workstation (Chenhua, Shanghai) at 298 K. The counter electrode, working electrode and reference electrode were a platinum plate, a mild steel sample and a saturated calomel electrode (SCE) with a Luggin capillary probe, respectively. The open circuit potential (OCP) corresponded to the corrosion potential reached in a quasi-stationary state after immersing the working electrode in 1 M HCl solution for 40 min. Electrochemical impedance spectroscopy (EIS) experiments were performed over a frequency range from 10^{-2} Hz to 10^5 Hz with amplitude of 5 mV at OCP. ZSimpWin software was used to fit the experimental data by an appropriate equivalent circuit. The potentiodynamic polarization curves were obtained with the potential range from -250 mV to 250 mV *vs.* OCP at a scan rate of 2 mV s^{-1}.

2.4. Morphology analysis

The surface morphologies of samples were captured by scanning electron microscopy (SEM) (Tescan Vega3 SEM). The acceleration voltage was 10 kV.

2.5. Computational details

The Gaussian 03W program was employed for quantum chemical calculations based on density functional theory (DFT). The geometry of the optimized structure of HBT was obtained by using the B3LYP functional with the 6-311++G(d, p) basis set [17, 18]. Furthermore, DFT was used to calculate the Mulliken charge, dipole moment (μ) and frontier molecular orbitals, including the energy of the highest occupied molecular orbital (E_{HOMO}), the energy of the lowest unoccupied molecular orbital (E_{LUMO}) and the energy gap ($\Delta E = E_{LUMO} - E_{HOMO}$) [15, 19].

The interaction between HBT and the Fe (110) surface was modeled in a simulation box (14.9 Å × 14.9 Å × 36.6 Å) under periodic boundary conditions by the Dmol3 program of Material Studio 7.0 software. A 4-layer 6×6 supercell (the lower two layers were constrained) with a 30 Å vacuum slab was used to simulate bulk metal. DFT calculations were treated within the generalized gradient approximation (GGA) function of Perdew-Burke-Ernzerhof (PBE). The displacement convergence, gradient, and tolerances of energy were 5×10^{-3} Å, 2×10^{-3} Ha Å^{-1} and 1×10^{-5} Ha, respectively. The interaction energy (E_{Fe-HBT}) between the Fe (110) surface and HBT followed the equation:

$$E_{Fe-HBT} = E_{Total} - E_{Fe} - E_{HBT} \qquad (1)$$

where E_{Total} is the energy of the Fe (110) surface and the adsorbed HBT molecule, E_{HBT} is the energy of the isolated HBT molecule and E_{Fe} is the energy of the steel surface, respectively.

3. RESULTS AND DISCUSSION

3.1. Weight loss measurements

The results of weight loss measurements were listed in Table 1. The corrosion rate (v), inhibition efficiency (η_w) and surface coverage (θ) were calculated by the following equations:

$$v = \frac{W}{St} \qquad (2)$$

$$\eta_w(\%) = \frac{v_0 - v}{v_0} \times 100 \qquad (3)$$

$$\theta = \frac{v_0 - v}{v_0} \qquad (4)$$

where W is the weight difference of samples, S is the total surface area of the samples, t is the immersion time and v_0 and v are the corrosion rates of the mild steel sample immersed in HCl without and with HBT, respectively.

The v decreased and η_w increased with the growing concentration of HBT, indicating that the HBT impeded the connection between the mild steel and the aggressive medium (Table 1). The inhibition efficiency increased to 92.9% with the concentration of HBT of 0.07 mM, suggesting that HBT is an attractive corrosion protector.

Table 1. Corrosion parameters obtained from weight loss tests for mild steel in 1 M HCl solution with and without (blank) various concentrations of HBT for 4 h at different temperatures.

Temperature (K)	Concentration (10^{-5} M)	v (g m^{-2} h^{-1})	η_w (%)	θ_w
298	Blank	4.5	/	/
	3	1.1	75	0.75
	4	0.79	82	0.82
	5	0.55	88	0.88
	7	0.19	96	0.96
308	Blank	7.3	/	/
	3	1.9	74	0.74
	4	1.4	81	0.81
	5	0.96	87	0.87
	7	0.39	95	0.95
318	Blank	17	/	/
	3	4.6	73	0.73
	4	3.4	80	0.80
	5	2.5	86	0.86
	7	1.2	93	0.93
328	Blank	23	/	/
	3	6.9	71	0.71
	4	5.2	78	0.78
	5	3.9	83	0.83
	7	2.1	91	0.91

According to Table 1, it can also be found that v increased and η_w decreased at various temperatures, probably because the high temperature can accelerate the adsorption rate of inhibitor molecules on the metal surface [20].

3.2. Potentiodynamic polarization curves

Fig. 2 shows the potentiodynamic polarization curves with and without HBT at 298 K. The corresponding electrochemical parameters including corrosion potential (E_{corr}), corrosion current density (i_{corr}), anodic Tafel slopes (β_a), cathodic Tafel slopes (β_c) and inhibition efficiency ($\eta_p\%$) are shown in Table 2. Herein β_a, β_c, and i_{corr} were gained from the extrapolation of anodic and cathodic lines to the corrosion potential. The $\eta_p\%$ is obtained from the following equation [20, 21]:

$$\eta_p\% = \frac{i^0_{corr} - i_{corr}}{i^0_{corr}} \times 100 \quad (5)$$

i^0_{corr} and i_{corr} are the corrosion current densities with and without inhibitors, respectively.

As shown in Fig. 2, both anodic and cathodic current density curves decreased with the increasing concentration of HBT, illustrating that both cathodic hydrogen evolution and anodic mild steel dissolution are inhibited. The improved inhibition efficiency was due to the adsorption property of HBT on the electrode surface.

The parallel cathodic polarization curves suggested that HBT would not change the hydrogen evolution mechanism and that it was still activation-controlled. As a result, the HBT molecules blocked the active sites of the steel surface. By contrast, the anodic polarization curves declined dramatically at lower overpotentials with the increasing concentration, which indicated that HBT inhibited steel corrosion through the formation of a protective film on the steel surface [22]. However, the current density displayed the opposite trend, because the desorption rate of HBT was higher than its adsorption rate due to the instant dissolution of Fe. Furthermore, when the potential was higher than -0.25 V, all of the anodic polarization curves were overlapped, meaning that the HBT molecules no longer exhibited an inhibition effect. This result demonstrated that the applied potential of the working electrode had a great influence on the adsorption mode of HBT.

Table 2. The potentiodynamic polarization parameters for mild steel in 1 M HCl solution in the absence and presence of different concentrations of HBT at 298 K.

Concentration (M)	E_{corr} (V *vs.* SCE)	i_{corr} (mA cm^{-2})	β_c (V dec^{-1})	β_a (V dec^{-1})	η_p (%)
0	-0.447	0.92	0.12	0.98	/
3×10^{-5}	-0.450	0.24	0.12	0.93	73.5
4×10^{-5}	-0.447	0.14	0.11	0.89	84.5
5×10^{-5}	-0.448	0.085	0.099	0.091	90.8
7×10^{-5}	-0.450	0.029	0.10	0.088	96.8

It can be ascertained from Table 2 that the maximal variation of E_{corr} was less than 85 mV, which suggested HBT was a mixed-type inhibitor by the influence of the steric hindrance effect [6]. As the

HBT concentration increased, the current density decreased. This indicates that the absorption strength and surface coverage were improved at high concentration. The changed values of β_a and β_c reflect that the cathodic and anodic corrosion rates were retarded by the absorption of HBT. The results from potentiodynamic polarization tests were consistent with the weight loss experiments.
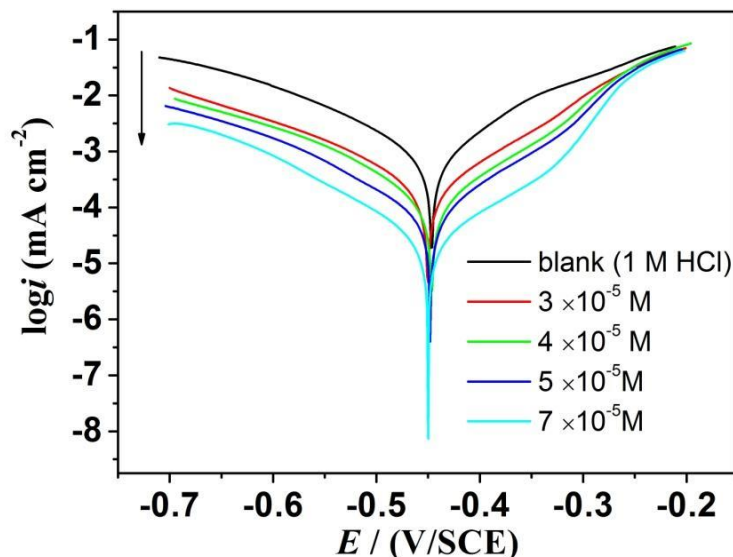

Figure 2. The potentiodynamic polarization curves for steel in 1 M HCl without and with various concentrations of HBT at 298 K.

3.3. EIS measurements

The Nyquist and Bode curves of mild steel in 1 M HCl solution with varied concentrations of HBT at 298 K are shown in Fig. 3. The shapes of Nyquist curves are similar, suggesting that the corrosion mechanism has not changed whether with or without the addition of HBT. Furthermore, the corrosion process of mild steel in the tested solution was mainly controlled by the charge transfer process [23]. Another reason for the deviation of Nyquist plots was the frequency dispersion arising from the roughness and inhomogeneity of the steel surface or interfacial effect. However, the diameter of these semicircles was significantly enhanced with the addition of HBT, which was attributed to the adsorption of HBT on the metal surface [24]. In the low frequency region of Bode plots (Fig. 3b), the higher concentration of HBT correlated with larger values of absolute impedance, which indicated that the inhibition efficiency of HBT was in positive correlation with concentration. Only one time constant of charge transfer can be found in Fig. 3c, which indicates the existence of a single constant phase element in the interface of metal and solution. Based on the characteristics of Nyquist and Bode plots, a simple Randles electrical equivalent circuit diagram (given in Fig. 4) was employed to model the metal/solution interface.

In Fig. 4, R_s is the solution resistance, R_{ct} is the charge transfer resistance, and CPE is the constant phase element. The impedance of the CPE is expressed as follows:

$$Z_{CPE} = \frac{1}{Y_0(j\omega)^n} \qquad (6)$$

where Y_0 is the CPE constant, n is the phase shift which can be explained as a degree of surface inhomogeneity, j is the imaginary unit and ω is the angular frequency. The electrochemical parameters obtained from experimental data are listed in Table 3. C_{dl} and $\eta_{EIS}\%$ are calculated from the following equations, respectively:

$$C_{dl} = (Y_0 R_{ct}^{1-n})^{1/n} \qquad (7)$$

$$\eta_{EIS}\% = \frac{R_{ct} - R_{ct}^0}{R_{ct}} \times 100 \qquad (8)$$

where R_{ct} and R_{ct}^0 are the charge transfer resistance with and without HBT, respectively.

In Table 3, the values of R_{ct} and $\eta_{EIS}\%$ increased with the rising concentration of HBT; instead, the values of C_{dl} decreased with the increasing concentration of HBT. Generally, the change in C_{dl} was related to the adsorption behavior of inhibitor molecules on the metal surface. The inhibitor molecules adsorbed at the metal/solution interface, which decreased the local dielectric constant and the thickness of the electrical double layer.
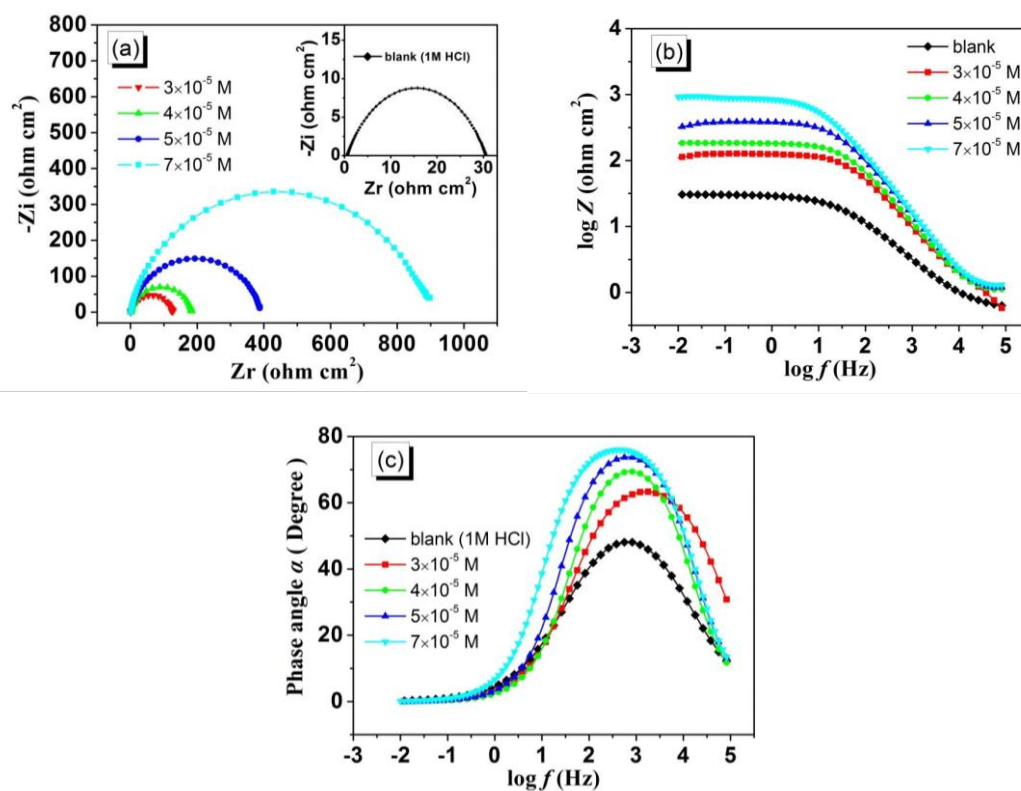

Figure 3. Nyquist (a) and Bode (b-c) plots for mild steel in 1 M HCl with various concentrations of HBT at 298 K.

The detailed explanations can be given by the Helmholtz model [25], which is depicted below:

$$C_{dl} = \frac{\varepsilon^0 \varepsilon}{d} S \qquad (9)$$

where ε is the local dielectric constant of the medium, ε^0 is the vacuum permittivity, S is the working electrode surface area and d is the thickness of the interfacial film. The inhibition efficiency values obtained from EIS tests were in good accordance with other tests.
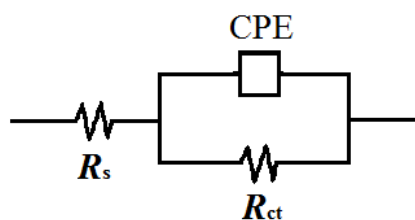

Figure 4. Electrical equivalent circuit used to fit the EIS experiment data.

Table 3. Impedance data for mild steel in 1 M HCl with various concentrations of HBT at 298 K.

C (M)	R_s (Ω cm^2)	CPE		R_{ct} (kΩ cm^2)	C_{dl} (mF cm^{-2})	η_{EIS} (%)
		Y_0 ($\times 10^{-7}$ S s^n cm^{-2})	n			
Blank	0.54	0.92	0.67	0.03	0.16	/
3×10^{-5}	0.43	0.11	0.77	0.13	0.031	76.37
4×10^{-5}	1.06	0.048	0.87	0.18	0.023	83.36
5×10^{-5}	1.12	0.030	0.89	0.37	0.017	91.94
7×10^{-5}	1.20	0.027	0.89	0.88	0.016	96.59

3.4. Adsorption isotherm and thermodynamic parameters

Generally, inhibition by organic molecules for metal is affected by the concentration of absorbed molecules on the steel surface. The Langmuir isotherm equation can provide the basic data of inhibitor-metal interaction. The data from weight loss tests are used to fit the optimum adsorption isotherm. For more accurate results, Temkin, Frumkin, Freundluich and Langmuir isotherms were employed to generate the results. The adsorption behavior of the studied inhibitor might be perfectly described by the Langmuir isotherm (Equation 10), with $R^2>0.999$.

$$\frac{C}{\theta} = \frac{1}{K_{ads}} + C \qquad (10)$$

where C is the concentration of inhibitor; θ is surface coverage; K_{ads} is the adsorptive equilibrium constant of inhibitor, which can be obtained from the intercept (1/K). The relationship between K_{ads} and ΔG^0_{ads} follows Equation 11. The thermodynamic parameters in Table 4 were obtained based on the Van 't Hoff equation (Equation 12), the plots (shown in Fig. 6) of lnK_{ads} versus $1/T$ and Equation 13.

$$K_{ads} = \frac{1}{55.5} \exp(\frac{-\Delta G^0_{ads}}{RT}) \qquad (11)$$

Here, 55.5 is the concentration of pure water (mol L^{-1}), T is adsorption temperature (K) and R is the gas constant (8.314 J K^{-1} mol^{-1}).

The linear regression coefficients were close to 1 in all cases, indicating that the adsorption of HBT on the steel surface was monolayer absorption. The higher value of K_{ads} means that the adsorption was stronger, and the negative value of ΔG^0_{ads} indicates that the process was spontaneous. The decrease in K_{ads} with the increase in temperature forecasted that the adsorption strength was weakening. The value of ΔG^0_{ads} was nearly -40 kJ mol^{-1}. Hence, the adsorption of HBT was determined by physical adsorption and chemical adsorption at lower temperature, while chemical adsorption showed the major effects at higher temperature [26]. The negative values of ΔH_{ads} pointed out that the adsorption processes were exothermic. Meanwhile, the negative values of ΔS^0_{ads} were known as the driving force of the adsorption process.

$$\ln K_{ads} = -\frac{-\Delta H^0_{ads}}{RT} + constant \qquad (12)$$

$$\Delta G^0_{ads} = \Delta H^0_{ads} - T\Delta S^0_{ads} \qquad (13)$$

Table 4. The thermodynamic parameters for mild steel in 1 M HCl solution with various concentrations of HBT at different temperatures.

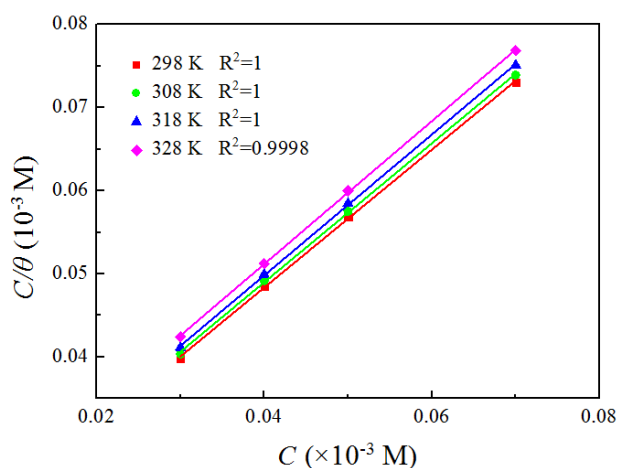| Temperature (K)	K_{ads} ($\times 10^4$ mol L^{-1})	ΔG^0_{ads} (kJ mol^{-1})	ΔH^0_{ads} (kJ mol^{-1})	ΔS^0_{ads} (kJ K^{-1} mol^{-1})
298	6.6	-37	-2.6	0.11
308	6.4	-38	-2.6	0.12
318	6.3	-39	-2.6	0.12
328	5.9	-40	-2.6	0.12

Figure 5. Langmuir isotherm plots for mild steel in 1 M HCl solution with various concentrations of HBT at different temperatures.
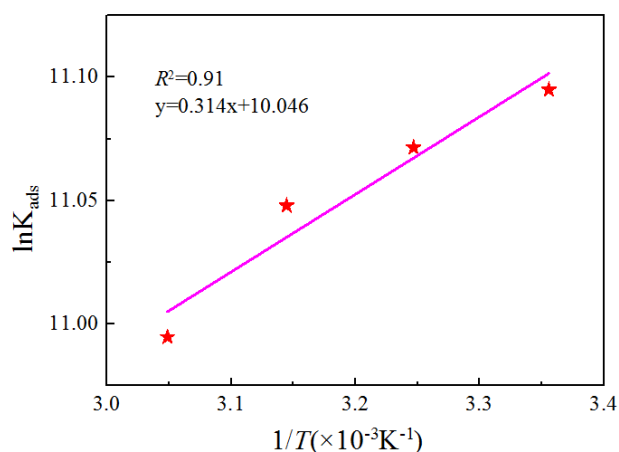
Figure 6. Van 't Hoff for mild steel in 1 M HCl solution.

3.5 Influence of temperature

The influence of temperature was also studied based on the weight loss test results. The plots of $\ln v$ versus $1/T$ and $\ln (v/T)$ versus $1/T$ fitted by Arrhenius equation (Equation 14) and transition state equation (Equation 15) are shown in Fig. 7 and Fig. 8.
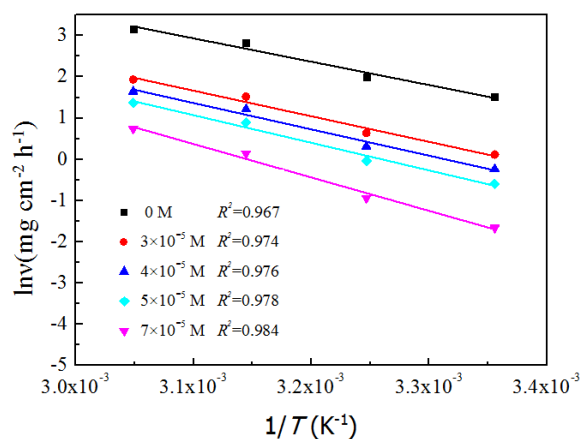

Figure 7. Arrhenius plots of $\ln v$ versus $1/T$ for mild steel in 1 M HCl solution with HBT at various concentrations.

The corrosion kinetic parameters, such as the apparent activation energy (E_a), the enthalpy of activation (H_a) and the entropy of activation (S_a), are calculated from the slopes and intercepts of curves.

$$\ln \upsilon = -\frac{E_a}{RT} + \ln A \qquad (14)$$

$$\ln \frac{v}{T} = \ln \frac{R}{nh} + \frac{\Delta S_a}{R} - \frac{\Delta H_a}{RT} \qquad (15)$$

Here, v is the corrosion rate, R is the gas constant, T is the thermodynamic temperature, A is the pre-exponential factor, h is the Planck constant and n is Avogadro's number.

The increasing E_a indicated that the dissolution of Fe became more difficult and that physical (electrostatic) adsorption occurred first. The changing trend of ΔH_a was the same as that of E_a. The competitive relationship between water and inhibitor molecules increased the degree of chaos on the surface of the steel, which was reflected in the increasing values of ΔS_a.
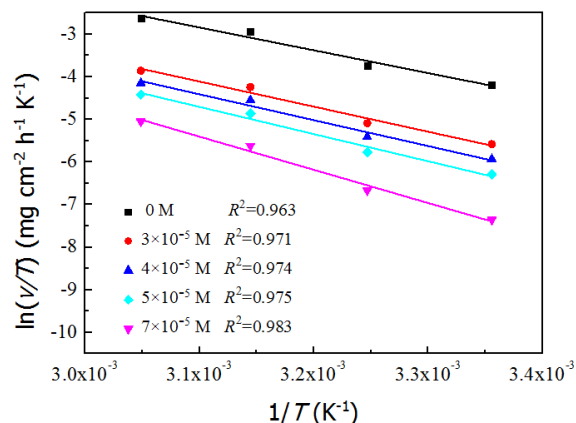

Figure 8. Arrhenius plots of ln (v/T) versus 1/T for mild steel in 1 M HCl solution with HBT at different concentrations.

Table 5. The corrosion kinetic parameters for mild steel in 1 M HCl solution containing different concentrations of HBT.

.

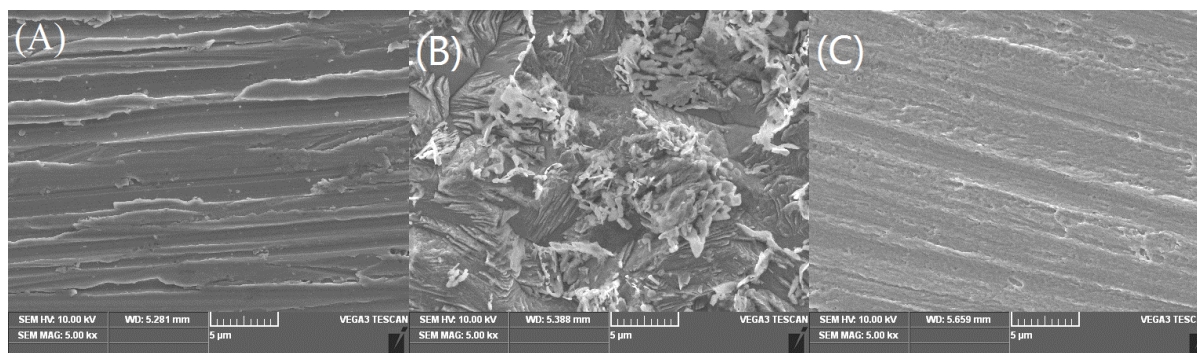| C (10^{-5} M)	E_a (kJ mol^{-1})	ΔH_a (kJ mol^{-1})	ΔS_a (J K^{-1} mol^{-1})
0	46	44	369
3	51	49	407
4	53	51	420
5	55	53	441
7	67	65	538

3.6. Morphological examination

Figure 9. SEM images of mild steel samples: fresh mild steel (A), and the specimens immersed in 1 M HCl solution without HBT (B) and with 0.07 mM HBT (C) at 298 K.

In Figure 9, the fresh mild steel showed a flat and smooth surface, while the sample immersed in aggressive solvent showed a roughness surface with large cracks. However, there were only negligible holes on the surface when adding HBT. This phenomenon confirmed that the absorbed HBT can prevent corrosion by forming a robust protective film even in the acidic solution.

3.7 Computational study

Furthermore, DFT calculations were used to reveal the adsorption and inhibition of HBT molecules. By comparison, the acidity coefficient (pK_a) of HBT displayed a higher value (~ 3.4) than the pH of 1 M HCl medium, proving the existence of HBT (HBT-H$^+$) protonated molecule. The HBT-H$^+$, together with neutral HBT molecule (HBT), was believed to play an important role during the process of inhibition corrosion. It is found that HBT-H$^+$ could remain stable by comparing the thermodynamic parameters with neutral HBT in Table 6. The electronic properties of HBT and HBT-H$^+$ were further investigated. The optimized geometry structure and frontier molecular orbitals (HOMO and LUMO) are shown in Fig. 10, and Table 7 shows the energy of HOMO (E_{HOMO}) and LUMO (E_{LUMO}), energy gap (ΔE) and molecular dipole moment (μ).

Table 6. The thermodynamic parameters of HBT and HBT-H$^+$.

	Energy (kcal mol^{-1})	Enthalpy (kcal mol^{-1})	Gibbs Free Energy (kcal mol^{-1})	Entropy (kca mol^{-1})
HBT-H$^+$	-1029.4	-1029.3	-1029.4	110.8
HBT	-1028.0	-1028.9	-1029.0	111.8

Temperature is 298 K; Pressure is 1 atm

It is generally known that HOMO is related to the ability of a molecule to donate electrons, and the higher E_{HOMO} value shows stronger electron-donating ability. Instead, LUMO is associated with the electron-accepting ability of a molecule, and a lower value of E_{LUMO} represents the strong electron-accepting ability[27]. As seen from Fig. 10b, the HOMO distributed around thiazole and aromatic rings, which would be the preferential sites for electrophilic attack. Conversely, the LUMO were delocalized around the rings (Fig. 10c), which indicated that the inhibitor could accept electrons of the steel surface through anti-bonding orbitals and form feed-back bonds. Table 7 displays the quantitative density distribution of frontier molecular orbitals around thiazole and aromatic rings. From Fig. 10 and Table 7, it can be seen that HBT and HBT-H$^+$ could equally adsorb onto the mild steel surface.

Table 7. The proportion of frontier orbitals around thiazole and aromatic rings

	HBT		HBT-H$^+$	
	HOMO	LUMO	HOMO	LUMO
thiazole ring	53.0%	57.0%	39.7%	63.7%
aromatic ring	46.7%	42.0%	51.1%	36.1%

In addition, the HOMO-LUMO gap (ΔE) is an important parameter to evaluate the stability of the inhibitor, and the lower value of ΔE indicates that the inhibitor molecule could more easily adsorb on the metal surface. As shown in Table 8, both HBT and HBT-H$^+$ have lower values of ΔE (4.62 eV, 3.93 eV, respectively), resulting in their strong ability to accept electrons from the *d*-orbital of steel as well as a high stability of the [Fe-L] complexes. By contrast, the HBT-H$^+$ exhibited higher reaction activity than HBT. At the same time, the dipole-dipole interaction between inhibitor and metal surface could improve the inhibition efficiency. Herein, the fact of $\mu_{HBT-H+} > \mu_{HBT}$ reflected the stronger adsorption between the HBT-H$^+$ and metal surface [28].

The ionization potential ($I = -E_{HOMO}$) and electron affinity ($A = -E_{LUMO}$) could be used to derive the electronegativity (χ) and global hardness (γ). The fraction of electron transfer (ΔN) between the inhibitor molecules and Fe surface is given by the following equation [29, 30]:

$$\Delta N = \frac{\chi_{Fe} + \chi_{inh}}{2(\gamma_{Fe} - \gamma_{inh})} \qquad (16)$$

where χ_{Fe} and γ_{Fe} are the absolute electronegativity and hardness of the Fe atom; χ_{inh} and γ_{inh} are the absolute electronegativity and hardness of the inhibitor molecules. A theoretical χ_{Fe} value of bulk Fe is 7 eV/mol, whereas γ_{Fe} is almost zero [30]. χ_{inh} and γ_{inh} are related to *I* and *A*.

$$\chi = \frac{I + A}{2} \qquad (17)$$

$$\gamma = \frac{I - A}{2} \qquad (18)$$

The direction of electron transfer is manifested by positive or negative ΔN values. From Table 8, HBT is the electron donor; instead, HBT-H$^+$ is the electron acceptor. It is noteworthy that the magnitude of the ΔN absolute value is not connected with inhibition efficiency [31].

Table 8. Quantum chemical parameters for HBT and HBT-H$^+$ by using the B3LYP/6-311 + + G(d,p) method.

	E_{HOMO} (eV)	E_{LUMO} (eV)	$\Box E$ (eV)	μ (Debye)	I (eV)	A (eV)	χ (eV)	$\Box \gamma$ (eV)	ΔN
HBT	-6.3	-1.7	4.6	1.8	6.3	1.7	4.0	2.3	0.66
HBT-H$^+$	-10.3	-6.3	3.9	2.4	10.3	6.3	8.3	2,0	-0.33

HBT and HBT-H$^+$ have been placed in a simulation box parallel with or perpendicular to the Fe(110) surface. The simulation results showed that both HBT and HBT-H$^+$ tended to adsorb in a parallel fashion onto the Fe(110) surface, as shown in Fig. 11(a, b). Namely, the thiazole and aromatic rings were the adsorption sites, which was in agreement with a previous report [1]. In addition, all of the hydrogen atoms were upturned after adsorption, which may be due to the hybridization between Fe and heavy atoms. The HBT-H$^+$ molecule is possibly a more efficient inhibitor because of its more negative adsorption energy (-0.634 eV) than that of HBT (–0.625 eV) [26, 27]. This is consistent with the analysis of weight loss and electrochemical measurements. From Fig. 11(c, d), the peaks of the state density of

HBT and HBT-H$^+$ were flat from -15 to 0 eV, also indicating the strong interaction between HBT or HBT-H$^+$ and the Fe(110) surface [32].
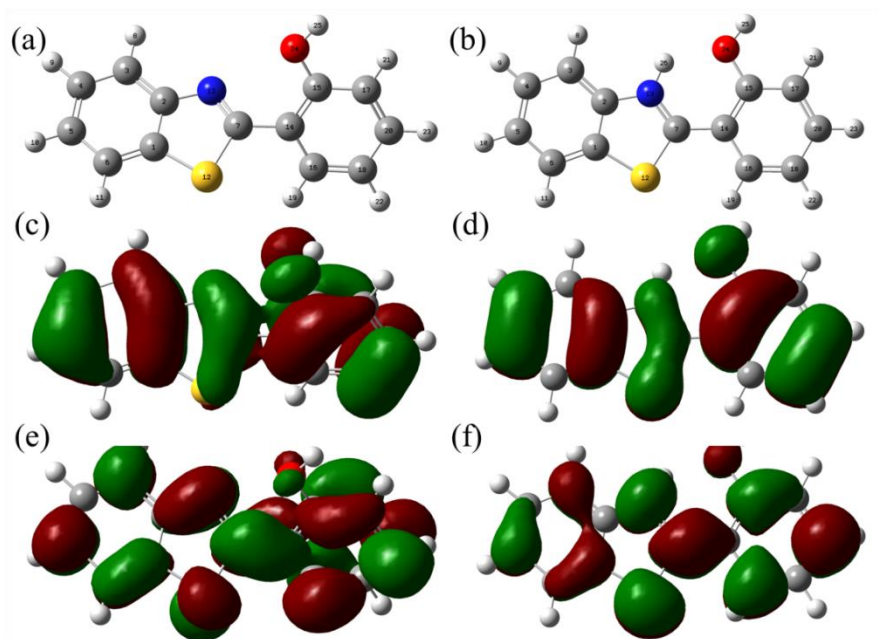

Figure 10. (a), (b) Optimized geometric structures of HBT and HBT-H$^+$ molecules: (c), (d) HOMO orbitals, (e), (f) LUMO orbitals, respectively.
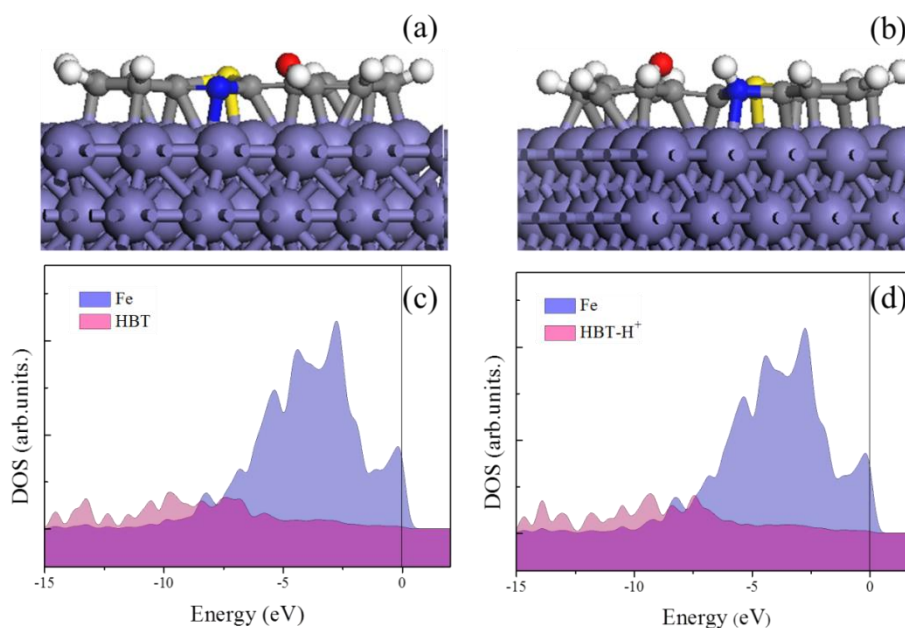

Figure 11. Stable adsorption configurations (side view) and density states projected for HBT and HBT-H$^+$ molecules on the Fe(110) surface.

3.8 Inhibition mechanism

According to the experimental results and theoretical calculations, the inhibition mechanism of HBT on mild steel in 1 M HCl can be described by the following steps and Fig. 12:

（i） The protonated HBT was formed by adsorbing a proton (H^+) via the lone pair electrons from N

（ii） The surface of mild steel is electropositive in the acidic environment. The Cl^- can easily stick, and thus, the electrical property of the steel surface was changed to electronegative. The protonated molecule ($HBT-H^+$) can adsorb onto the steel surface by electrostatic forces.

（iii） $HBT-H^+$ chemisorbed onto the steel surface through coordinate bonds.
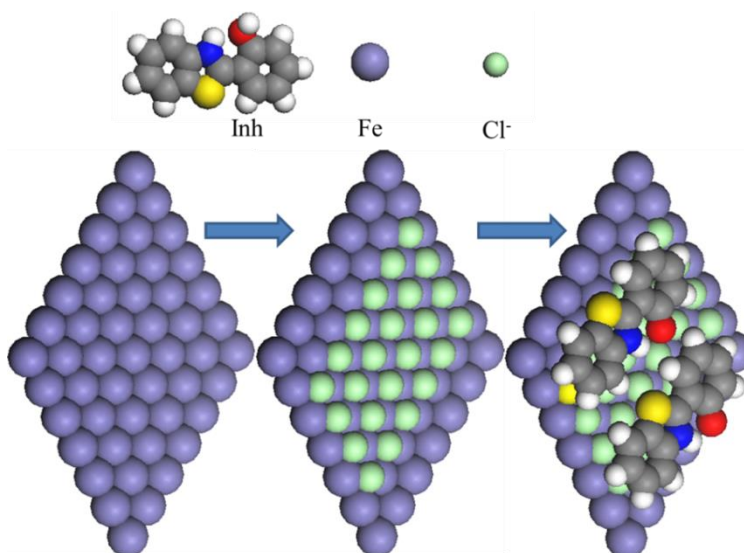
（iv）

Figure 12. Intuitive schematic of the mechanism of inhibition

4. CONCLUSION

In this work, we found a promising organic compound corrosion inhibitor for mild steel in 1 M HCl. The inhibition performance was tested by physical, chemical and electrochemical methods. The theoretical calculations were also performed to reveal the inhibition mechanism of HBT. The detailed results are demonstrated as follows:

1) The results of weight loss experiments and electrochemical tests indicated that HBT is an efficient inhibitor of mild steel in 1 M HCl. They also showed that the inhibition efficiency increased with the growing concentration of HBT and that the optimal concentration of HBT is 0.07 mM. 2) The values of charge transfer resistance increased in the presence of HBT in EIS tests, which indicated that HBT can protect steel from corrosion by forming a robust film. The Tafel plots illustrated that HBT is a mixed-type inhibitor. 3) The adsorption process of HBT obeys the Langmuir adsorption isotherm. 4) SEM showed that the surface is smooth in the presence of the inhibitor due to the protective film. 5) The

results of theoretical calculations explained that the protective film was formed by the electrostatic forces between the protonated HBT and electronegative surface.

References

1. X.W. Zheng, S.T. Zhang, W.P. Li, L.L. Yin, J.H. He and J.F. Wu, *Corrosion Science*, 80 (2014) 383.
2. P. Singh and M.A. Quraishi, *Measurement*, 86 (2016) 114.
3. J.H. Tan, L. Guo, T.M. Lv and S.T. Zhang, *International Journal of Electrochemical Science*, 10 (2015) 823.
4. L. Guo, S.H. Zhu and S.T. Zhang, *Journal of Industrial and Engineering Chemistry*, 24 (2015) 174.
5. J. Zhang, L. Zhang, G. Tao and N. Chen, *International Journal of Electrochemical Science*，13 (2018) 8645.
6. D.K. Singh, S. Kumar, G. Udayabhanu and R.P. John, *Journal of Molecular Liquids*, 216 (2016) 738.
7. I. Ukpong, O. Bamgboye and O. Soriyan, *International Journal of Corrosion*, 2018 (2018).
8. I. Milosev, N. Kovacevic, J. Kovac and A. Kokalj, *Corrosion Science*, 98 (2015) 107.
9. M. Shahraki, M. Dehdab and S. Elmi, *Journal of the Taiwan Institute of Chemical Engineers*, 62 (2016) 313.
10. M. Gholami, I. Danaee, M.H. Maddahy and M. RashyandAvei, *Industrial & Engineering Chemistry Research*, 52 (2013) 14875.
11. L. Guo, S.T. Zhang, T.M. Lv and W.J. Feng, *Research on Chemical Intermediates*, (2013).
12. S.S. Abd El Rehim, S.M. Sayyah, M.M. El-Deeb, S.M. Kamal and R.E. Azooz, *International Journal of Industrial Chemistry*, 7 (2016) 39.
13. T.L.P. Galvao, A. Kuznetsova, J.R.B. Gomes, M.L. Zheludkevich, J. Tedim and M.G.S. Ferreira, *Theoretical Chemistry Accounts*, 135 (2016).
14. A. Rahimi and S. Amiri, *Journal of Polymer Research*, 23 (2016) 1.
15. D. Gustincic and A. Kokalj, *Physical Chemistry Chemical Physics*, 17 (2015) 28602.
16. N. Kovačević and A. Kokalj, *Corrosion Science*, 73 (2013) 7.
17. A.D. Becke, *The Journal of Chemical Physics*, 98 (1993) 5648.
18. A.D. Becke, *Journal of Chemical Physics*, 98 (1993) 5648.
19. A. Kokalj, S. Peljhan, M. Finsgar and I. Milosev, *Journal of the American Chemical Society*, 132 (2010) 16657.
20. R. Solmaz, *Corrosion Science*, 79 (2014) 169.
21. D. Daoud, T. Douadi, H. Hamani, S. Chafaa and M. Al-Noaimi, *Corrosion Science*, 94 (2015) 21.
22. M. Yadav, S. Kumar, I. Bahadur and D. Ramjugernath, *International Journal of Electrochemical Science*, 9 (2014) 3928.
23. M. Deyab, *Desalination*, 439 (2018) 73.
24. C.N. Unnisa and S. Chitra, *Journal of Environmental Chemical Engineering*, 6 (2018) 6714.
25. R. Haldhar, D. Prasad and A. Saxena, *Journal of environmental chemical engineering*, 6 (2018) 5230.
26. I. B. Obot and N. O. Obi-Egbedi, *Corrosion Science*, 52 (2010) 282.
27. N.O. Obi-Egbedi, I.B. Obot and M.I. El-Khaiary, *Journal of Molecular Structure*, 1002 (2011) 86.
28. N.O. Obi-Egbedi and I. B. Obot, *Corrosion Science*, 53 (2011) 263.
29. R.G. Pearson, *Journal of the American Chemical Society*, 85 (1963) 3533.
30. R.G. Pearson, *Inorganic Chemistry*, 27 (1988) 734.

Int. J. Electrochem. Sci., Vol. 14, 2019

31. L. Guo, X.L. Ren, Y. Zhou, S.Y. Xu, Y. Gong and S.T. Zhang, *Arabian Journal of Chemistry*, 10 (2017) 121.
32. L. Guo, S. Zhu, W. Li and S.T. Zhang, *Asian Journal of Chemistry*, 27 (2015) 2917.